Advances in Applied Mathematics and Mechanics
Adv. Appl. Math. Mech., Vol. **2**, No. 5, pp. 573-586

DOI: 10.4208/aamm.10-10S04
October 2010

Lattice Boltzmann and Finite Volume Simulation of Inviscid Compressible Flows with Curved Boundary

Kun Qu[1], Chang Shu[1,*] and Yong Tian Chew[1]

[1] *Department of Mechanical Engineering, National University of Singapore, 10 Kent Ridge Crescent, Singapore, 119260*

Received 16 April 2010; Accepted (in revised version) 25 April 2010
Available online 13 July 2010

Abstract. A 2D lattice Boltzmann model for inviscid compressible flows was proposed in this paper. Finite volume method was implemented on 2D curvilinear structural grids to solve the lattice BGK-Boltzmann equations. MUSCL scheme was used to perform interpolation. The obtained results agree excellently well with experimental and previous numerical results.

AMS subject classifications: 76P05

Key words: Lattice Boltzmann method, compressible flow, finite volume method, structural grids.

1 Introduction

As a promising method, the lattice Boltzmann method (LBM) has been widely studied in the last decades. Although LBM was derived from the lattice gas automata (LGA), it can also be derived from the continuous Boltzmann equation and it is a special finite difference form of the discrete velocity Boltzmann equation (DVBE). DVBE can be solved with finite difference method, finite volume method or finite element method. The solution of DVBE by the FVM was first conducted by Nannelli and Succi [1,2].

FVM is a method based on the weak solution of PDE and it has the feature of keeping conservation laws of physics. Due to this feature, it is a primary approach in simulations of compressible flows with discontinuities, such as shock waves and contact discontinuities. Many FVM schemes were proposed and widely used to capture discontinuities, such as TVD, MUSCL, ENO/WENO. So it is natural to use such FVM schemes to solve DVBE to simulate compressible flows with discontinuities.

*Corresponding author.
URL: `http://serve.me.nus.edu.sg/shuchang/`
Email: kunqu@coe.pku.edu.cn (K. Qu), mpeshuc@nus.edu.sg (C. Shu), mpecyt@nus.edu.sg (Y. T. Chew)

However, in the history of LBM, its applications were limited to incompressible flows. This is because LB models were derived based on low Mach number expansion of Maxwellian function [3–6]. Although some compressible LB models were proposed [7–10], the Mach number range of them is small and no supersonic numerical results were published. At the same time, some of them have many free parameters. To overcome these difficulties, we proposed a 2D model for inviscid compressible flows, D2Q13L2 (L2 means two energy-levels) in [12] from a circular function. Based on this model, we solved DVBE with the 2nd order TVD FVM on uniform rectangular grids to simulate several cases of compressible flows [11,12]. Our simulations have shown that it can simulate supersonic flows with high Mach number and strong shock waves. Based on our research, Li et al. [13] and Wang et al. [14] proposed their double ditribution function LB models for viscous compressiblel flows.

In this work, we extended the application of the D2Q13L2 model to cuvilinear structural grids to simulate flow fields with irregular boundaries. The MUSCL scheme with the smooth limiter was used to capture discontinuities. The implementation of boundary conditions for compressible flows was discussed. In order to validate the method, we simulated several test problems and compared the results with experimental data or previous results. Excellent agreement was obtained. The rest of this paper was organized as follows. Section 2 will introduce our D2Q13L2 model. Section 3 will present the FVM discretization of DVBE. Section 4 is about implementations of boundary conditions. Numerical applications will be presented in Section 5. Finally, Section 6 concludes the present work.

2 D2Q13L2 model for 2D inviscid compressible flows

The detailed derivation of the D2Q13L2 model was presented in [11,12]. Here, we only briefly describe it. First, our derivation is not based on Maxwellian function which is complicate and difficult to mathematically mannipulate. Alternatively, we proposed a simplified function. For 2D problems, the form of the simplified function is

$$g=\begin{cases}\dfrac{\rho}{2\pi c}, & \text{if } \|\boldsymbol{\xi}-\boldsymbol{u}\|=c\equiv\sqrt{D\,(\gamma-1)\,e}\\ & \quad\text{and } \lambda=e_p=\Big[1-\dfrac{D}{2}(\gamma-1)\Big]e,\\ 0, & \text{else,}\end{cases}\tag{2.1}$$

where $\boldsymbol{\xi}$ is particle velocity, λ is rest energy of particles, c is an effective peculiar velocity, $\boldsymbol{u}$ is the mean flow velocity, e is the mean internal energy, γ is the specific heat ratio of the gas, D is the space dimension. This function means that all mass, specific momentum and energy concentrate on a circle located in a 3D space of ξ_x-ξ_y-λ (as shown in Fig. 1). Although this function is very simple, it satisfies all needed statistical relations to make BGK DVBE recover the compressible NS equations.

Second, based on this circular function, we discretized it onto some fixed points in the 3D space of ξ_x-ξ_y-λ to construct a LB model. We adopted the Lagrangian interpolation to assign the circular function onto a set of discrete points without small Mach

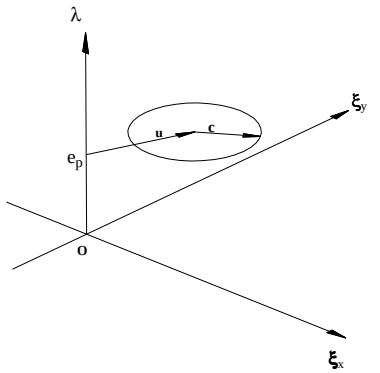

Figure 1: The schematic of the circular function g_s. It is located on a plane $\lambda = e_p$ in the ξ_x-ξ_y-λ space. **u** is the mean velocity and **c** is the effective peculiar velocity.

number assumption. In the ξ_x-ξ_y-λ space, there are $\alpha = 1, \cdots, N$ discrete points, $\boldsymbol{e}_\alpha$. We will discretize the circular function onto all $\boldsymbol{e}_\alpha$. For any $d\rho$ on the circle, we assign $d\rho$ onto every $\boldsymbol{e}_\alpha$ with a weight function $\varphi_\alpha(\boldsymbol{\xi}, \lambda)$. Thus, the accumulated density on $\boldsymbol{e}_\alpha$ is

$$\rho_\alpha = \frac{\rho}{2\pi c} \oint \varphi_\alpha(\boldsymbol{\xi}, \lambda) \mathrm{d}s. \tag{2.2}$$

Here, we have a question. If ρ_α were used as f_α^{eq}, what conditions do $\varphi_\alpha(\boldsymbol{\xi}, \lambda)$ have to satisfy? By analyzing the statistical relations needed to make BGK DVBE recover the compressible Euler equations, we can obtain that $\varphi_\alpha(\boldsymbol{\xi}, \lambda)$ is a set of Lagrangian interpolation polynomials of 3rd order in $\boldsymbol{\xi}$ and 1st order in λ. A 3rd order Lagrangian interpolation stencil $\varphi_\alpha(\boldsymbol{\xi})$ in 2D space was first constructed. The configuration of the stencil is the same as D2Q13 lattice velocity model. After the locations of the nodes in velocity space are known, the complete lattice can be constructed by splitting the 13 nodes onto two energy-level (λ_0 and λ_1).Thus a 26-nodes stencil and the base

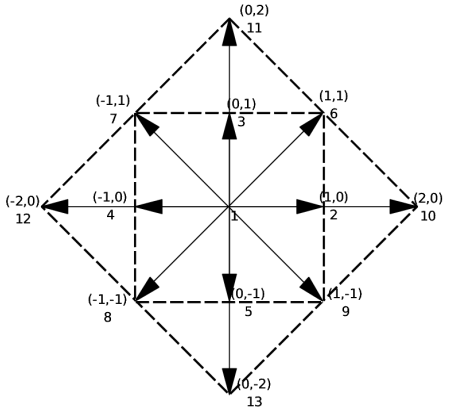

Figure 2: The scheme of D2Q13 lattice.

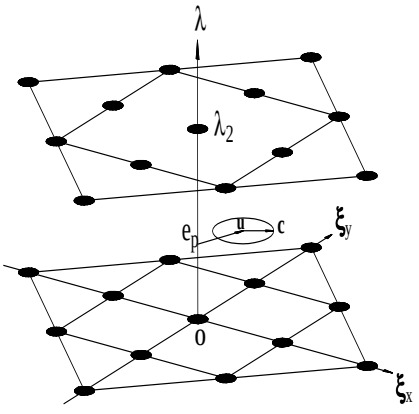

Figure 3: D2Q13L2 lattice.

polynomials

$$\begin{cases} \varphi_{\alpha 1}(\boldsymbol{\xi},\lambda) = (1-\lambda)\varphi_\alpha(\boldsymbol{\xi}), & \text{for energy level } \lambda_1 = 0, \\ \varphi_{\alpha 2}(\boldsymbol{\xi},\lambda) = \lambda\varphi_\alpha(\boldsymbol{\xi}), & \text{for energy level } \lambda_2 > e_p, \end{cases} \tag{2.3}$$

are obtained. With the assigning function $\varphi_\alpha(\boldsymbol{\xi},\lambda)$, the equilibrium functions, $f^{eq}_{\alpha v}$, can be given by

$$f^{eq}_{\alpha v} = \frac{\rho}{2\pi c}\oint \varphi_{\alpha v}(\boldsymbol{\xi},\lambda)\mathrm{d}s, \tag{2.4}$$

where $v = 1, 2$. Due to the simplicity of the circular function, Eq. (2.4) can be integrated analytically. The procedure of the above derivation can be done with a short Maple script. The formulars of f^{eq}_α are presented in [12].

3 FVM formulations

Since we use FVM to solve DVBE in curvilinear grids, we write BGK DVBE as the conservative form in 2D general coordinates

$$\frac{\partial \hat{f}_k}{\partial t} + \frac{\partial \hat{F}_k}{\partial \xi} + \frac{\partial \hat{G}_k}{\partial \eta} = \hat{\Omega}_k, \tag{3.1}$$

note that ξ and η are the generalized coordinates of the curvilinear grid. k is the index of the distribution function. And

$$\hat{f}_k = \frac{f_k}{J}, \quad \hat{F}_k = \frac{f_k e_{k\xi}}{J}, \quad \hat{G}_k = \frac{f_k e_{k\eta}}{J}, \quad \hat{\Omega}_k = -\frac{f_k - f^{eq}_k}{\tau J}, \tag{3.2}$$

where

$$J = \begin{vmatrix} \dfrac{\partial\xi}{\partial x} & \dfrac{\partial\xi}{\partial y} \\ \dfrac{\partial\eta}{\partial x} & \dfrac{\partial\eta}{\partial y} \end{vmatrix}, \qquad \begin{cases} e_{k\xi} = \xi_x e_{kx} + \xi_y e_{ky}, \\ e_{k\eta} = \eta_x e_{kx} + \eta_y e_{ky}, \end{cases} \qquad \begin{cases} \xi_x = J y_\eta, \\ \xi_y = -J x_\eta, \\ \eta_x = -J y_\xi, \\ \eta_y = J x_\xi. \end{cases} \tag{3.3}$$

The semi-discretized form of Eq. (3.1) is

$$\frac{1}{J}\frac{\partial f_{k,i,j}}{\partial t} = -\left[\hat{F}_{k,i+\frac{1}{2},j} - \hat{F}_{k,i-\frac{1}{2},j}\right] - \left[\hat{G}_{k,i,j+\frac{1}{2}} - \hat{G}_{k,i,j-\frac{1}{2}}\right] - \hat{\Omega}_{k,i,j}, \tag{3.4}$$

where i and j are indices of a cell, $\hat{F}_{k,i\pm1/2,j}$ and $\hat{G}_{k,i,j\pm1/2}$ are numerical fluxes on the interfaces of a cell (i, j). They can be computed with a Riemann solver. For Eq. (3.1), the exact Riemann solver is available and cheap since the convective terms are linear. $\hat{F}_{k,i+1/2,j}$ for instance, can be given as

$$\hat{F}_{k,i+\frac{1}{2},j} = \begin{cases} (f_L)_{k,i+\frac{1}{2},j}\left(\dfrac{e_{k\xi}}{J}\right)_{i+\frac{1}{2},j} & \text{if } e_{k\xi} \geq 0 \\ (f_R)_{k,i+\frac{1}{2},j}\left(\dfrac{e_{k\xi}}{J}\right)_{i+\frac{1}{2},j} & \text{if } e_{k\xi} \leq 0 \end{cases} \tag{3.5}$$

where f_L and f_R are the distribution functions just on the left and right side of the interface $(i+1/2, j)$. In this work, they are determined by the third order MUSCL with the smooth limiter to extrapolate the value of f_α^n on the two sides of an interface

$$\begin{cases} (f_L)_{k,i+\frac{1}{2},j} = f_{\alpha,i,j} + \left\{ \frac{s}{4} \left[(1-\kappa s)\,\Delta_- + (1+\kappa s)\,\Delta_+ \right] \right\}_i , \\ (f_R)_{k,i+\frac{1}{2},j} = f_{\alpha,i+1,j} - \left\{ \frac{s}{4} \left[(1-\kappa s)\,\Delta_+ + (1+\kappa s)\,\Delta_- \right] \right\}_{i+1} , \end{cases} \tag{3.6}$$

where $\kappa = 1/3$ and s is the Van Albada limiter [15]

$$s = \frac{2\Delta_+\Delta_- + \varepsilon^2}{\Delta_+^2 + \Delta_-^2 + \varepsilon}.$$

Here ε is a small number (we set ε=10^{-6}) preventing division by zero in region of null gradient and

$$(\Delta_+)_i = f_{k,i+1,j} - f_{k,i,j}, \qquad (\Delta_-)_i = f_{k,i,j} - f_{k,i-1,j}.$$

With $(f_L)_{i+1/2}$ and $(f_R)_{i+1/2}$, the numerical flux on the interface $i+1/2$ can be computed according to the exact Riemann solver, Eq. (3.5). Computing $\hat{\Omega}_{k,i,j}$ is easy when a full explicit time scheme is applied for time advancement. However, in order to resolve the dimensionless relaxation time τ, the time step Δt should be small enough as compared to τ value.

In this work, the Euler forward scheme is applied for the temporal discretization. Although it is a first order explicit scheme, it is good enough not only for steady flows but also for many unsteady problems since the time step Δt is limited by τ, making the CFL number very small.

As the lattice of the LB model is fixed, the problems to be simulated should be normalized to the scale of the lattice. So, dimensionless equations should be used. There are three independent reference variables, reference density ρ_{ref}, length L_{ref} and internal energy e_{ref} (note that, this e_{ref} is not a discrete velocity vector). The other reference and dimensionless variables are defined as follows

$$\begin{aligned} &U_{ref} = \sqrt{e_{ref}}, && t_{ref} = \frac{L_{ref}}{U_{ref}}, && \breve{t} = \frac{t}{t_{ref}}, \\ &\breve{x} = \frac{x}{L_{ref}}, && \breve{\rho} = \frac{\rho}{\rho_{ref}}, && \breve{e} = \frac{e}{e_{ref}}, \\ &\breve{\tau} = \frac{\tau}{t_0}, && \breve{\lambda}_2 = \frac{\lambda_2}{e_{ref}}, && \breve{u} = \frac{u}{U_{ref}}, \end{aligned}$$

where $\breve{\tau}$ is the Knudsen number and is very small for inviscid flows (we set $\breve{\tau} = 10^{-4} \sim 10^{-3}$). So the dimensionless time step is seriously limited (for example, $\Delta\breve{t} = 1/4\breve{\tau}$). The value of e_{ref} is very important. It determines U_{ref} and normalizes e to $\breve{e}$

from which $\check{c}$ is computed. In order to make sure that the circle is located inside the lattice to avoid extrapolation, we need

$$|\check{\mathbf{u}}| + \check{c} < \sqrt{2},$$

where $\sqrt{2}$ is the shortest distance from the original point to the edges of the D2Q13 lattice. Therefore e_0 should be big enough. Determining this parameter is easy and it has a clear physical and mathematical meaning. For safety, e_{ref} can be set a little bit greater than the maximum specific stagnation internal energy, $\max(e_0)$, in the whole flow field. Also, λ_2 should be big enough. In our simulations, we set $\lambda_2 = e_{ref}$ for simplicity. So $\check{\lambda}_2 = 1$ and we have the following relations

$$\begin{cases} \check{\rho} = \sum\limits_{i=1}^{13}\sum\limits_{v=1}^{2} f_{iv}^{eq}, \\ \check{\rho}\check{u} = \sum\limits_{i=1}^{13}\sum\limits_{v=1}^{2} f_{iv}^{eq}\mathbf{e}_i, \\ \check{\rho}\check{E} = \sum\limits_{i=1}^{13}\Big[\sum\limits_{v=1}^{2} f_{iv}^{eq}\dfrac{\mathbf{e}_i^2}{2} + f_{i2}^{eq}\Big], \end{cases} \quad \text{and} \quad \begin{cases} \check{e} = \check{E} - \dfrac{\check{u}^2}{2}, \\ \check{p} = (\gamma-1)\check{\rho}\check{e}. \end{cases}$$

4 Boundary conditions

In our simulations in this work, many boundary conditions are involved, such as subsonic inlet/outlet, supersonic inlet/outlet and adiabatic inviscid wall boundary conditions. For all the boundary conditions, we can use the following way to implement them. At first, we need to determine mean flow variables (ρ, u, v and e) on the boundary using available means of traditional CFD. Then, we can compute f_{iv}^{eq} on the boundary according to ρ, u, v and e. Since inviscid flows are considered and viscous effects (viscous stress, heat conduction and work done by viscous stress) are negligible, the non-equilibrium part of f_i which results in the viscous effects, can be neglected. This guarantees that the use of f_{iv}^{eq} on the boundary is accurate enough.

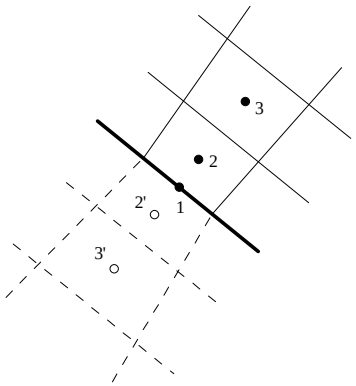

Figure 4: Implementation of slip wall condition. The thick line is the wall, cells drew with thin solid lines are cells in fluid domain and cells drew with dashed lines are ghost cells inside the wall.

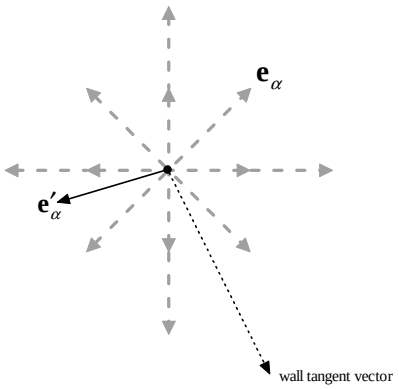

Figure 5: Reflection-projection method for the inviscid wall boundary condition.

We also implement the slip adiabatic wall boundary condition with a reflection-projection method. On a rectangular grid, it is easy to perform the specular reflecting operation to implement slip-wall condition because every velocity has its mirror peer. However, this is not the case for curvilinear grids. We have a little more work to do for the curvlinear gird. Fig. 4 shows the wall and the nearby cells. The thick line is the wall, cells drew with thin solid lines are cells in the fluid domain. In order to determine the distribution function in the ghost cell $2'$, we first reflect every velocity $\mathbf{e}_\alpha$ in cell 2 to its mirror velocity, $\mathbf{e}'_\alpha$. Usually, the reflected velocity $\mathbf{e}'_\alpha$ is not coincident with any node in the D2Q13L2 lattice (Fig. 5). So we assign (project) its distribution function $f_{\alpha v}$ onto all the nodes of the D2Q13L2 lattice. And the accumulated value on the velocity $\mathbf{e}_j$, $f_{jv}(2')$ is

$$f_{jv}(2') = \sum_{\alpha=1}^{13} f_{\alpha v}(2)\varphi_j\left(e'_{\alpha x}, e'_{\alpha y}\right).$$

This projection can keep conservation of moments (mass, momentum, convective flux of momentum and energy) of the reflected psudo-particles. So, the projected distribution functions have the same physical meaning with the reflected distribution functions. With the same method, the distribution function $f_{jv}(3')$ in the ghost cell $3'$ can be determined. After that, the flux through the wall can be computed with MUSCL scheme. It is not difficult to prove that this reflection-projection operation satisfies the inviscid wall condition and is of the second order accuracy.

This assigning method might be also used to impose boundary conditions of symmetric plane and specular-reflection in curvilinear grids.

5 Numerical results

This section presents numerical results of some test cases. All these numerical tests will verify that our deriving method, models, numerical procedure and implementation of boundary conditions.

5.1 Flow past a bump in a channel

First, we consider a flow in the GAMM channel [16] (Fig. 6) which has a 10% circular bump ($h = 0.1$) in it. The inflow Mach number is 0.675. Fig. 7 shows the computational grid of 80×22.

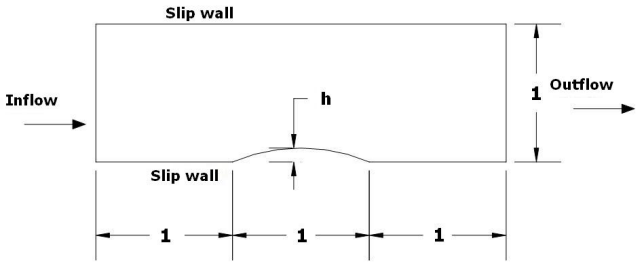

Figure 6: Schematic view of the GAMM channel.

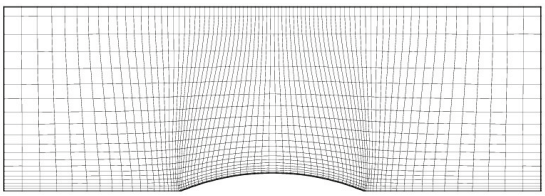

Figure 7: The structural curvilinear grid of channel with bump of 10%.

In the computation, total energy $e_0 = 1.96$ for $u = 0.675$ and $\rho = 1$ of $Mach = 0.675$. The reference variables are

$$\rho_{ref} = 1, \qquad L_{ref} = h, \qquad \breve{\tau} = 10^{-3},$$
$$e_{ref} = 2 > \max(e_0) = 1.96, \quad \Delta\breve{t} = \frac{\breve{\tau}}{4}.$$

The left boundary is subsonic inlet, the right boundary is set as extrapolating outflow, the top and bottom boundaries are slip adiabatic walls. The computed Mach number contour is shown in Fig. 8. Fig. 9 shows the Mach number profiles on the walls. The solid dot line in this figure is the result computed by solving Euler equation with WENO scheme [17]. Obviously, the present results agree well with those obtained by the Euler solver.

5.2 Flows around Rae2822 airfoil

Two simulations were performed for this case. For the first one, $M_\infty = 0.75$ and $\alpha = 3^\circ$, while for the second one, $M_\infty = 0.729$ and $\alpha = 2.31^\circ$. In these simulations, a 225×65 C-type grid was used. The boundary conditions are shown in Fig. 10 in which the outer boundary is about 20 times of the chord length far from the airfoil.

In the computation, for the freestream with $u_\infty = Ma$ and $\rho_\infty = 1$, the internal

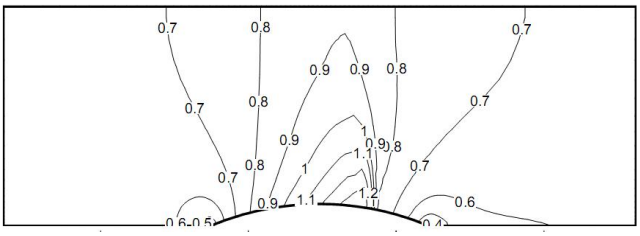

Figure 8: Mach number contour of $M = 0.675$ flow in the channel of 10%.

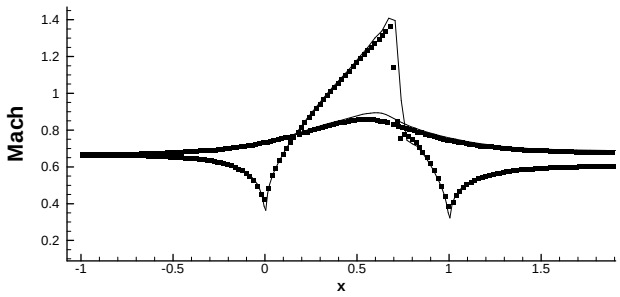

Figure 9: Distribution of Mach number along walls.

energy can be determined as

$$e_\infty = \frac{p_\infty}{(\gamma-1)\rho_\infty} = \frac{1/\gamma}{(\gamma-1)\times 1} = \frac{1}{\gamma(\gamma-1)}.$$

Then the total energy e_0 can be obtained according to the Mach number

$$e_0 = \left(1 + \frac{\gamma-1}{2}\right) Ma^2.$$

The reference variables are $\rho_{ref} = 1$, $L_{ref} =$ chordlength, $e_{ref} > \max(e_0)$ and $\check{\tau} = 10^{-3}$, $\Delta\check{t} = \check{\tau}/4$.

The pressure contours of the first simulation are shown in Fig. 11. The shock wave is captured clearly. And the pressure coefficient profile is presented in Fig. 12 in which the results computed with the same grid by solving Euler equations with Jameson's central scheme [18] are shown as solid symbols. Obviously, the two results agree excellently well.

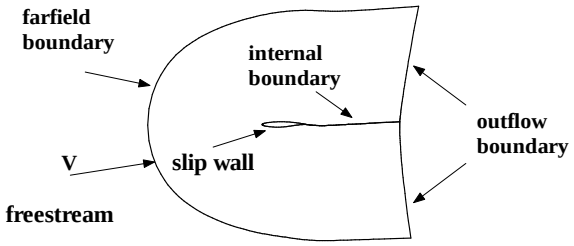

Figure 10: Boundary conditions of flow around Rae2822 airfoil.

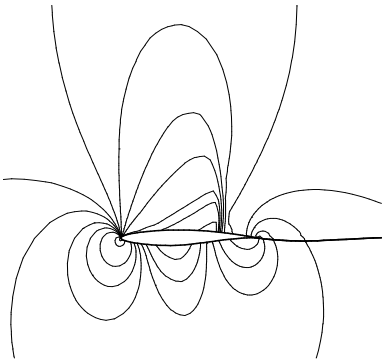

Figure 11: Pressure contours of flow over Rae2822 airfoil ($M_\infty = 0.75$ and $\alpha = 3^\circ$).

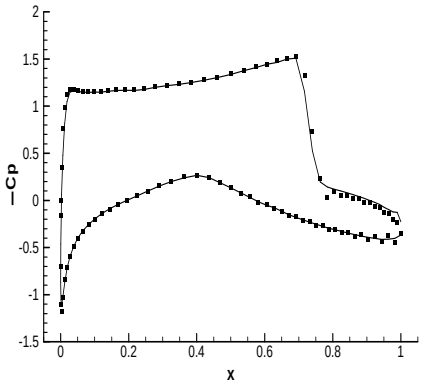

Figure 12: Pressure coefficient profiles of flow over Rae2822 airfoil ($M_\infty = 0.75$ and $\alpha = 3^\circ$).

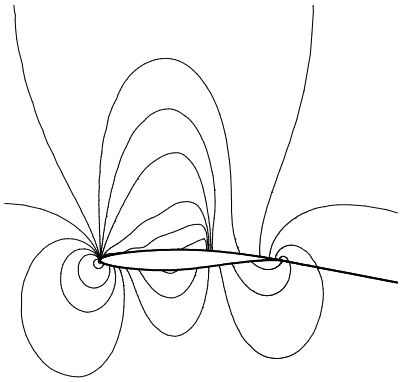

Figure 13: Pressure contours of flow over Rae2822 airfoil ($M_\infty = 0.729$ and $\alpha = 2.31^\circ$).

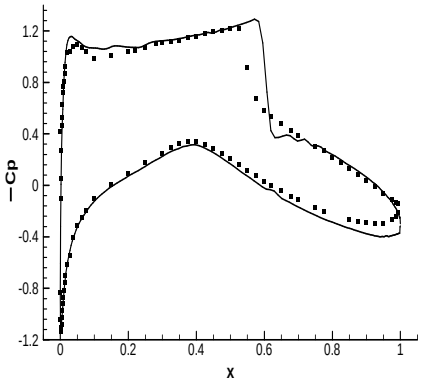

Figure 14: Pressure coefficient profiles of flow over Rae2822 airfoil ($M_\infty = 0.729$ and $\alpha = 2.31^\circ$).

For the second simulation, the pressure contours and pressure coefficient profiles are shown in Figs. 13 and 14 respectively. The solid dots in Fig. 14 are the experimental data [19] which have some deviations from our results because the flow in the experiment is a turbulent flow in which the shock wave interacts with the boundary layers. Therefore, its stiffness and location are different from those of the numerical inviscid simulation.

5.3 Supersonic flow over a two dimensional cylinder

Finally, supersonic flow over a cylinder is simulated for two different Mach numbers ($M_\infty = 3, 5$). A 61×81 mesh, shown in Fig. 15, was generated analytically [20] by

$$\begin{cases} x = -\big(R_x - (R_x - 1)\xi\big)\cos\big(\theta(2\eta - 1)\big), \\ y = \big(R_y - (R_y - 1)\xi\big)\sin\big(\theta(2\eta - 1)\big), \end{cases} \tag{5.1}$$

where $R_x = 3$, $R_y = 6$ and $\theta = 5\pi/12$, while ξ and η change from 0 to 1. The flow field is initialized according to the free-stream state, while reflection wall conditions

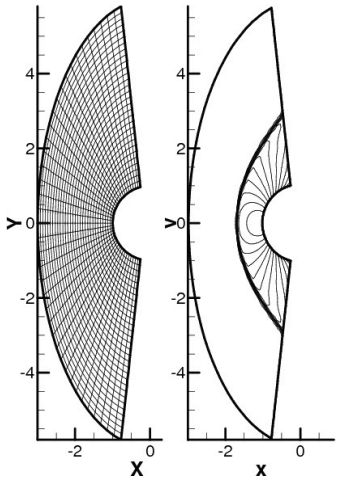

Figure 15: Mach 3 flow around a cylinder: grid and pressure contours.

are imposed at the surface of the cylinder. On the two supersonic outflow boundaries, extrapolating method is applied.

The contours of pressure for $M_\infty = 3$ are plotted in Fig. 15. Although the pressure jump is very large, the shock wave is captured without spurious oscillations. Fig. 16 shows the profile of pressure along the central line, as well as the result computed from the sixth order compact-Roe scheme with the adaptive filter by Visbal & Gaitonde [21]. Our profile agrees excellently well with theirs. It is noticed that the shock we simulated smears over 3 cells and our profile is not as sharp as the reference data. This is because the grid used by Visbal & Gaitonde [21] is finer (101×81 in the upper-half domain) than the present work and their sixth order scheme is much more accurate than the third order MUSCL scheme we used here.

For the higher free-stream Mach number case, simulation of flows around blunt bodies with Roe scheme may produce the so-called "carbuncle" [22] which ruins the

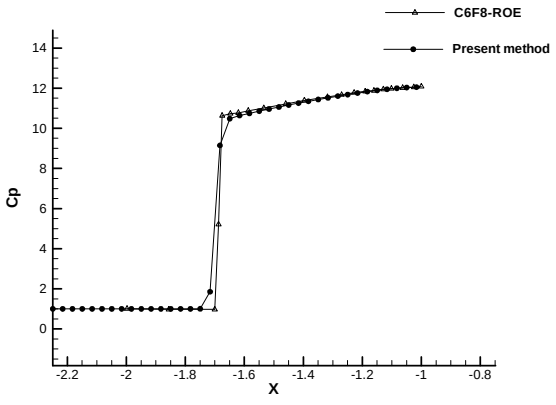

Figure 16: Pressure coefficient profile along the central line for Mach 3 flow around a cylinder.

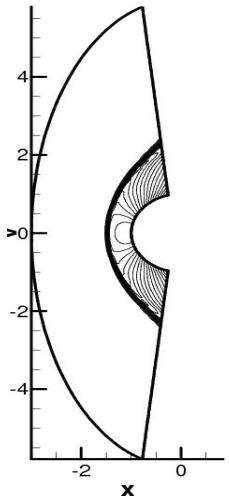

Figure 17: Pressure contour of Mach 5 flow around a cylinder.

bow shock waves. Some special treatments such as entropy fixing are needed to fix this problem. The "carbuncle" phenomenon doses not occur in our LBM simulation (Fig. 17). The pressure profile and reference data [21] are shown in Fig. 18. The location of the shock wave agrees excellently well with the semi-empirical value [23] and the result by Visbal & Gaitonde [21]. Since a much finer grid (201×121 in the upper-half domain) was used in [21], our shock wave is smeared as compared to the data extracted from [21].

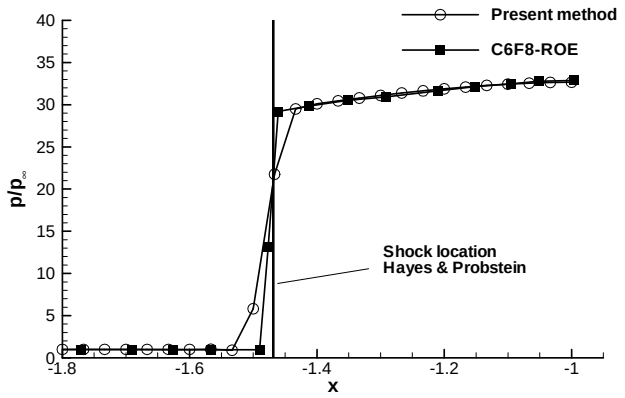

Figure 18: Pressure coefficient profile along the central line for Mach 5 flow around a cylinder.

6 Conclusions

In this work, the D2Q13L2 model is extended to simulate compressible inviscid flows on general curvilinear coordinate system. D2Q13L2 model is not derived from the

conventional Maxwellian distribution functions. Instead, it is derived from the simple circular function. It can allow the adjustment of specific heat ratio. The conventional FVM is applied to solve the discrete velocity Boltzmann equation. Since the system is linear, the exact Riemann solver can be used. In addition, an interpolation scheme is proposed to implement the slip boundary condition on the solid wall. All the numerical examples demonstrate that the proposed D2Q13L2 model can effectively simulate compressible inviscid flows with curved boundaries.

References

[1] R. BENZI, S. SUCCI AND M. VERGASSOLA, *The lattice Boltzmann equation: theory and application*, Phys. Rep., 222 (1992),145–197.

[2] F. NANNELLI AND S. SUCCI, *The lattice Boltzmann equation in irregular lattices*, J. Stat. Phys., 68 (1992), 401–407.

[3] X. Y. HE AND L. S. LUO, *Theory of the lattice Boltzmann method: from Boltzmann equation to the lattice Boltzmann equation*, Phys. Rev. E., 56 (1997), 6811–6817.

[4] X. Y. HE AND L. S. LUO, *A priori derivation of the lattice Boltzmann equation*, Phys. Rev. E., 55 (1997), R6333–R6336.

[5] X. Y. HE, S. Y. CHEN AND G. D. DOOLEN, A novel thermal model for the lattice Boltzmann method in incompressible limit, J. Comput. Phys., 146 (1998), 282–300.

[6] H. W. ZHENG, C. SHU, Y. T. CHEW AND J. QIU, *A platform for developing new lattice Boltzmann models*, Int. J. Mod. Phys. C., 16 (2005), 61–84.

[7] G. W. YAN, Y. S. CHEN AND S. X. HU, *Simple lattice Boltzmann model for simulating flows with shock wave*, Phys. Rev. E., 59 (1999), 454–459.

[8] W. P. SHI, S. Y. WEI AND R. W. MEI, *Finite-difference-based lattice Boltzmann method for inviscid compressible flows*, Numer. Heat. Tr. B-Fund., 40 (2001), 1–21.

[9] T. KATAOKA AND M. TSUTAHARA, *Lattice Boltzmann method for the compressible Euler equations*, Phys. Rev. E., 69 (2004), 056702-1.

[10] T. KATAOKA AND M. TSUTAHARA, *Lattice Boltzmann method for the compressible Navier-Stokes equations with flexible specific-heat ratio*, Phys. Rev. E., 69 (2004), 035701-1.

[11] K. QU, C. SHU AND Y. T. CHEW, *Simulation of shock-wave propagation with finite volume lattice Boltzmann method*, Int. J. Mod. Phys. C., 18 (2007), 447-454.

[12] K. QU, C. SHU AND Y. T. CHEW, *Alternative method to construct equilibrium distribution functions in Lattice-Boltzmann method simulation of inviscid compressible flows at high Mach number*, Phys. Rev. E., 75 (2007), 036706.

[13] Q. LI, Y. L. HE, Y. WANG AND W. Q. TAO, *Coupled double-distribution-function lattice Boltzmann method for the compressible Navier-Stokes equations*, Phys. Rev. E., 76 (2007), 056705.

[14] Y. WANG, Y. L. HE AND Q. LI, *Lattice Boltzmann model for viscous compressible flows with high Mach number*, Proceedings of First Asian Symposium on Computational Heat Transfer and Fluid Flow, Xi'an, China, 2007.

[15] G. D. VAN. ALBADA, B. VAN LEER AND W. W. ROBERTS, *A comparative study of computational methods in cosmic gas dynamics*, Astron. Astrophys., 108 (1982), 76–84.

[16] A. RIZZI AND H. VIVIAND, Numerical Methods for the Computation of Inviscid Transonic Flows with Shock Waves, Wieweg and Sohn, Braunschweig/Wiesbaden, 1981.

[17] J. FÜRST, *A weighted least square scheme for compressible flows*, Flow. Turbul. Combust., 76 (2006), 331–342.

[18] A. MEISTER, Transonic flow past a RAE 2822 profile (2D), http://www-ian.math.uni-magdeburg.de/anume/testcase/euler/euler1-e.html, 2000.
[19] P. H. COOK, M. A. MCDONALD AND M. C. P. FIRMIN, Aerofoil RAE 2822-Pressure Distributions and Boundary Layer and Wake Measurements, AGARD Report AR 138, 1979.
[20] G. S. JIANG AND C. W. SHU, *Efficient implementation of weighted ENO schemes*, J. Comput. Phys., 126 (1996), 202–228.
[21] M. R. VISBAL AND D. V. GAITONDE, *Shock capturing using compact-differencing-based methods*, 43rd AIAA Aerospace Sciences Meeting and Exhibit; Reno, NV; USA; 10-13 Ja. 2005. AIAA-2005-1265, 2005.
[22] D. GAITONDE AND J. SHANG, *Accuracy of flux-split algorithms in high-speed viscous flows*, AIAA. J., 31 (1993), 1215–1221.
[23] W. HAYES AND R. PROBSTEIN, Hypersonic Flow Theory, Volume 1, Academic Press, New York, 1959.